ORIGINAL MANUSCRIPT

Trans-dichlorooxovandium (IV) complex as a novel photoinducible DNA interstrand crosslinker for cancer therapy

Kumar Somyajit[1,4,†], Bhabatosh Banik[2,5,†], Sneha Saxena[1], Sharath Babu[1], Manoor Prakash Hande[3], Akhil R.Chakravarty[2,*] and Ganesh Nagaraju[1,*]

[1]Department of Biochemistry, Indian Institute of Science, Bangalore 560012, India, [2]Department of Inorganic and physical Chemistry, Indian Institute of Science, Bangalore 560012, India and [3]Department of Physiology, NUS Yong Loo Lin School of Medicine, Singapore

[4]Present address: NNF Center for Protein Research, University of Copenhagen, Faculty of Health and Medical Sciences, DK-2200, Copenhagen N.
[5]Present address: Department of Chemistry, University of Gerogia, Athens, GA 30602, USA

*To whom correspondence should be addressed. Tel: +91 80 22933055. Fax: +91 80 23600814; E-mail: nganesh@biochem.iisc.ernet.in
†These authors contributed equally to this work.

Correspondence may also be addressed to Akhil R.Chakravarty. Tel: +91 80 22932533; Fax: +91 80 23600683; E-mail: arc@ipc.iisc.ernet.in

Abstract

Although DNA interstrand crosslinking (ICL) agents such as mitomycin C, cisplatin and psoralen serve as potent anticancer drugs, these agents are known to have dose-limiting toxic effects on normal cells. Moreover, tumor resistance to these agents has been reported. Here, we show that *trans*-dichlorooxovanadium (IV) complex of pyrenyl terpyridine (VDC) is a novel photoinducible DNA crosslinking agent. By a combination of *in vitro* and *ex vivo* experiments including plasmid-based assays, we find that VDC forms monoadducts on the DNA and can be activated by UV-A and visible light to generate DNA interstrand crosslinks. VDC efficiently activates Fanconi anemia (FA) pathway of DNA interstrand crosslink repair. Strikingly, photoinduction of VDC induces prolonged activation of cell cycle checkpoint and a high degree of cell death in homologous recombination (HR)/ICL repair defective cells. Moreover, VDC specifically targets cells that express pathological RAD51C mutants. These data imply that VDC can be potentially used for cancer therapy and suggest that tumors arising in patients with gene mutations in FA and HR repair pathway can be specifically targeted by a photoactivatable VDC.

Introduction

Eukaryotic cells are continuously faced with a myriad of genotoxic assaults that constantly threaten the integrity of the genome (1,2). Cellular DNA is susceptible to multiple chemical modifications by the products of endogenous metabolic processes or by various environmental agents and chemotherapeutic drugs that cause various types of lesions in the DNA (3). These DNA lesions, if unrepaired, can subsequently drive the cells towards apoptosis or may lead to mutations, thus paving the path to tumorigenesis (1,3,4).

Among many types of DNA damage, DNA interstrand crosslinks (ICLs), which can covalently link the two strands of duplex DNA, is considered as most dangerous DNA lesions (5). As separation of the two strands of DNA is essential for cellular processes of replication and transcription, ICLs act as a pronounced block for cell growth, and are specifically detrimental to rapidly proliferating cells (5,6). Different crosslinking drugs such as cisplatin, mitomycin C (MMC) and psoralens induce DNA crosslinks by distinct mechanisms (5,7). These agents require a

Abbreviations

DSB	double strand break
FA	Fanconi anemia
HR	homologous recombination
ICL	interstrand crosslinking
MMC	mitomycin C
NER	nucleotide excision repair
PBS	phosphate-buffered saline
PDT	photodynamic therapy
VDC	trans-dichloro oxovanadium (IV) complex of pyrenyl terpyridine
XPB	xeroderma pigmentosum complementation group B

loss of two chemically active groups from the drug molecule, so as to react with bases on each DNA strand. Crosslinking agents can covalently connect two nucleotide residues either on the same DNA strand (intrastrand crosslink) or on opposite strands (interstrand crosslink) (7). Whereas intrastrand crosslinks can be readily removed by the nucleotide excision repair (NER) mechanism, ICLs are more dangerous DNA lesions and can indeed lead to cell death if left unrepaired. However, deliberate induction of ICLs is a proven strategy for the treatment of cancer (5,8) and hyper proliferative skin disorders including psoriasis (9). Thus, ICL agents are being widely used as potential anticancer drugs for the treatment of various types of cancer.

Cells have evolved with various mechanisms to repair toxic DNA lesions and thereby protect the integrity of genome (10–12). Investigations from Fanconi anemia (FA) patients revealed a bonafide pathway for the repair of ICLs in S-phase in higher eukaryotes (vertebrates) (13). FA is a rare chromosome instability genetic disorder characterized by congenital abnormalities, progressive bone marrow failure and susceptibility to cancer (14). The hallmarks of FA cells are extreme sensitivity to ICLs and chromosome instability in the form of radial chromosomes and chromatid breaks, which is widely used as a classic diagnostic test for FA (13). In addition, when exposed to ICL agents, FA cells exhibit G2/M accumulation due to the defect in the repair of ICLs (5). The FA pathway of ICL repair occurs predominantly in S-phase and involves the concerted actions of translesion DNA synthesis (TLS), NER and homologous recombination (HR) (5). To date, studies carried out in different laboratories over more than a decade identify about 19 genes (*FANC A, B, C, D1, D2, E, F, G, I, J, L, M, N, O, P, Q, R, S and T*) which play a critical role in the FA pathway of ICL repair (15,16). The proteins encoded by these genes form a heterogeneous pool of factors either directly involved in DNA repair or in cell signaling in response to DNA damage. Thus, FA pathway provides an important link between DNA damage signaling and repair (15). FA pathway is activated when the replication fork encounter ICL lesion. In response to ICL induced replication arrest, FANCM is recruited to the sites of ICL damage which in turn recruits the FA core complex (FANCA, B, C, E, F, G and L) to monoubiquitinate FANCD2–FANCI complex. This stabilizes the FANCD2–FANCI heterodimer at the sites of damage and the monoubiquitinated complex serves as a docking site for the recruitment of subsequent repair factors such as TLS polymerases, NER machinery and HR proteins to complete ICL repair (17,18). In response to ICLs, ATR-CHK1 pathway arrests the cells in the S/G2 phase to facilitate crosslink repair. Interestingly, five of the FA genes *FANCD1*, *FANCJ*, *FANCN*, *FANCO* and *FANCS* are identified as breast cancer susceptibility (*BRCA*) genes *BRCA2*, *BACH1*, *PALB2*, *RAD51C* and *BRCA1*, respectively, highlighting the crucial role of the pathway in maintenance of genome integrity and prevention of tumorigenesis (18).

The significant advances in understanding of ICL repair over the past decade has led to the rapid development and use of novel ICL agents for effective killing of cancer cells (5). However, the therapeutic potential of these agents are markedly limited by the dose limiting toxicity of ICLs to normal cells (5,19), and in particular, the damage caused to the haematopoietic system (20). Circumventing this toxicity is expected to reduce side effects in patients, thus providing opportunities for developing new ICL-based chemotherapeutic agents. Another major challenge faced by usage of ICL-based agents is the occurrence of acquired/inherited drug resistance among tumors (19). Indeed, tumor resistance has been detected in ovarian and testicular tumors following chronic exposure to high doses of cisplatin (21,22). To overcome these limitations, extensive studies are in progress for the design of photoactivatable DNA crosslinkers as a novel approach for cancer chemotherapy (23–25). Photoactivation offers potential for initiating unusual ligand substitution and redox reactions of transition metal complexes, and may offer new strategies for the development of anticancer agents (26). Several conventionally used clinical drugs including cisplatin, melphalan and MMC are known to form ICLs constitutively, whereas ICL induction by psoralen requires UV-A irradiation (5). Given the toxic effect of constitutive induction of ICLs on the normal cells, and the side effects of constant UV-A irradiation for psoralen activation during cancer therapy (27), there is an importunate need to develop an alternative potent photoinducible ICL agents.

In this study, we have synthesized and characterized a novel photoinducible DNA crosslinking agent *trans*-dichlorooxovanadium (IV) complex of pyrenyl terpyridine (VDC-visible light inducible DNA crosslinker). We show that VDC forms monoadduct with DNA in dark, which upon activation by UV-A and visible light, enables formation of DNA interstrand crosslinks. VDC efficiently activates FA pathway of ICL repair. Strikingly, photoinduction of VDC induces prolonged activation of cell cycle checkpoint and high degree of cell death in FA pathway defective cells. Moreover, VDC specifically targets cells that express pathological RAD51C mutants. These data suggests that VDC can be potentially used as a novel photoinducible anticancer agent.

Materials and methods

Cell lines and cell culture

HeLa, U2OS and MCF7 human cells were obtained from ATCC and cultured as described (28). I-BR3 (primary human fibroblasts) cells were kindly provided by Dr Penny Jeggo and cultured as described (28). Xeroderma pigmentosum complementation group B (XPB) patient cells were kindly provided by Dr Manoor Prakash Hande. pcDNA3βeGFP plasmid was kindly provided by Dr Ralph Scully. Chinese hamster lung fibroblast cells CL-V4B (RAD51C$^{-/-}$) and V79B (parental) cells were kindly provided by Dr Malgorzata Z. Zdzienicka and grown as described (29). The authentication of CL-V4B (RAD51C$^{-/-}$) was previously performed as described (30) and was re-authenticated by RAD51C immunoblotting and mitomycin C sensitivity (29). CL-V4B cells stably expressing wild-type (wt) and RAD51C mutants from pcDNA3β vector were generated as described previously (29). The cells were maintained in Dulbecco's Modified Eagle's Medium, supplemented with 10% fetal bovine serum, 100 IU/ml of penicillin, 100 μg/ml of streptomycin and 2 mM Glutamax at 37°C in a humidified incubator at 5% CO_2. Adherent cultures were grown as monolayer and passaged once in 4–5 days by trypsinizing with 0.25% Trypsin-EDTA (29). Δ*uvrD E. coli* strain was kindly provided by Dr Susan Rosenberg.

Western blot and antibodies

Cells were harvested and lysed in RIPA buffer supplemented with complete protease and phosphatase inhibitor mixture (Roche Applied Science). Proteins were resolved on 7.5 or 10% SDS-PAGE and transferred onto PVDF membranes (Millipore). Membranes were blocked using 5%

milk or 3% BSA in TBST (50 mM Tris–HCl, pH 8.0, 150 mM NaCl, 0.1% Tween 20) and incubated with primary antibody for 1–10 h. The primary antibodies against H2AX, Lamin A, α-tubulin, RAD51, CHK1P (Ser-345), FANCD2, and β-actin used for western blot analysis were purchased from Santa Cruz Biotechnology. γ-H2AX antibody was obtained from BD Biosciences. Membranes were incubated with secondary antibody for 1 h and later developed by chemiluminescence and captured using ChemiDoc (GE LAS 4000) (28,29,31).

G2/M accumulation assays

Cells were treated (or untreated) with the indicated concentrations of cVDC and VDC complexes or MMC followed by recovery in the fresh media for 24 h. Treated cells were trypsinized, and single cells were fixed overnight with 70% ethanol in phosphate-buffered saline (PBS) at –20°C. After centrifugation cells were incubated with 0.1 mg/ml RNase A (Fermentas) in PBS at 42°C for 4 h and then incubated for 10 min with 50 µg/ml propidium iodide in the dark. A total of 10^4 cells were analyzed by Canto flow cytometer (BD Biosciences). Aggregates were gated out, and a percentage of cells with 4N DNA content was calculated using FACSDiva Version 6.1.1software (BD Biosciences) (29).

Immunofluorescence

Exponentially growing HeLa cells were seeded onto cover slips and then treated (or untreated) with the indicated concentrations of cVDC and VDC complexes or MMC. After treatment, the cells were washed with PBS and fixed in 4% formaldehyde. The cells were then permeabilized with 0.5% Triton X-100 for 15 min and blocked in 1% BSA for 30 min. The cells were incubated with the indicated primary antibodies and fluoresceinisothiocyanate (FITC)-conjugated secondary antibodies (Sigma) for 1 h each at room temperature and then stained with PI before mounting onto slides. Cells were acquired using a Carl Zeiss confocal microscope, and images were processed using Zeiss LSM image browser software (29).

Cell survival assays

Cells were seeded onto 24-well plates at a density of 5000 cells per well in triplicate and were allowed to adhere for 4–6 h. Cells were treated with complexes cVDC and VDC for 6 h in dark. Later, cells were irradiated with UV-A (365 nm, 678 mJ/s. m^2 with UVITEC LF 206LS lamp for 30 min) or visible light for (400–700 nm, 10 J/cm^2 for 1 h). Cells were later recovered in the fresh media and incubated for 36 h. Subsequently, 500 µl of 0.5 mg/ml MTT (Sigma) labelling reagent was added to each well, and the cultures were incubated for 4 h at 37°C in dark. Medium was removed, and 500 µl of DMSO was added to the cells; 100 µl of the resulting mixture was transferred to a 96-well plate and analyzed using microplate reader (VersaMax ROM Version 3.13). In a parallel experiment, cell survival was measured by colony formation assay. Cells (200) were seeded onto 60 mm petridish in duplicate and then treated with cVDC and VDC complexes at indicated concentration. After 6 h in dark, cells were later irradiated with UV-A (365 nm, 30 min) or visible (400–700 nm, 1 h) light. Later, cells were recovered in the fresh media and incubated for 8 days and stained with crystal violet. Colonies containing ~50 cells were counted as one colony. Percent growth was calculated as treated cells/untreated cells × 100 (29).

Alkaline agarose gel electrophoresis assay

To test DNA–DNA crosslinking ability of tested compounds, we carried out photoactivation of complexes followed by alkaline agarose gel electrophoresis. pUC19 plasmid DNA was linearized by *BamHI* restriction endonuclease. The DNA crosslinking experiment was performed in phosphate buffer (pH7.5). Samples were exposed to UV light (365 nm) at room temperature. The crude reaction mixtures were resolved on a 0.8% denaturing alkaline agarose gel. The gel was subsequently stained in an ethidium bromide solution (10 µg/ml ethidium bromide solution in 1 M Tris–1.5 M NaCl buffer at pH = 7.5) for 1 h. Gels were visualized by UV and captured using gel documentation system (G:boxSyngene).

Comet assays

The modified alkaline comet assay was performed to detect genome-wide DNA crosslink formation. About 20 000 cells were incubated with ICL complexes for 6 h in dark. Later, treated cells were irradiated with UV-A or visible light for 1 h; cells were harvested and alkaline comet assay was performed. Harvested cells were mixed with 150 µl of 0.5% low melting point agarose (Sigma) and spread on agarose precoated frosted microscopic glass slides. Cells were lysed by placing slides in cold lysis solution (2.5 M sodium chloride, 100 mM EDTA, 10 mM TrisHCl, pH 10, 1% Triton X-100, 10% DMSO) for 2 h. After lysis, slides were washed with PBS and incubated for 1 h in alkaline unwinding buffer (300 mM NaOH and 1 mM EDTA, pH 13) in the dark at 4°C and later electrophoresed in the same buffer for 1 h at 25V and 300 mA at 4°C. Slides were neutralized in 0.4 M Tris–HCl (pH 7.5) and stained with ethidium bromide for analysis. Image of at least 50 cells per sample were captured using a fluorescence microscope (Olympus IX 71), and tail moment was quantified using comet score (29).

Cell fractionation and chromatin extraction

Chromatin extraction was performed to quantitate the presence of vanadium using ICP-MS as a measure of intact complex onto the chromatin. HeLa cells after treatment with the complexes were harvested and chromatin fractionation was carried out. The cytosolic protein fraction was removed by incubation in hypotonic buffer (10 mM HEPES, pH 7, 5 mM NaCl, 0.3 M sucrose, 0.5% Triton X-100, supplemented with protease inhibitor; Roche) for 15 min on ice and centrifuged at 1500 g for 5 min. The soluble nuclear fraction was removed by incubation with nuclear buffer (10 mM HEPES, pH 7, 200 mM NaCl, 1 mM EDTA, 0.5% NP-40 and protease inhibitor cocktail) for 10 min on ice and then centrifuged at 13 000 rpm for 2 min. The pellets were resuspended in lysis buffer (10 mM HEPES, pH 7, 500 mM NaCl, 1 mM EDTA,1% NP-40 and protease inhibitor cocktail), sonicated at low amplitude, and centrifuged for 1 min at 13 000 rpm; the supernatant was then transferred to a new tube. Total chromatin protein was quantified using the standard Bradford method, and 50 µg of protein was used to detect vanadium on the chromatin. In parallel, cellular uptake and stability of complexes was determined by detecting vanadium from whole cell lysate (29).

Results

Design and synthesis of novel photoactivatable oxovanadium (IV) complexes

Extensive studies are in progress for the design of novel photoactivatable metallo-drugs for cancer chemotherapy. Photoactivation offers potential for initiating unusual ligand substitution and redox reactions of transition metal complexes. Moreover, photoactivatability of such agents would offer controlled action specifically at the tumor site and at a desired point of time. In this study, we have synthesized oxovanadium (IV) complexes of suitably modified terpyridine ligands of the formulation *trans*-[VOCl$_2$(R-tpy)] (cVDC (control VDC) and VDC) where R-tpy is (4′-phenyl)-2,2′:6′,2″-terpyridine (ph-tpy in cVDC) and (4'-pyrenyl)-2,2′:6',2″-terpyridine (py-tpy in VDC) (Figure 1A and B). Apart from being a bioessential metal and cofactor for various metalloenzymes, vanadium (IV) possesses a low energy absorption band in the spectral range of 630–800 nm which enables complexes of vanadium (IV) to undergo photoredox processes and subsequent ligand exchange reactions upon irradiation with low energy visible light. Such ligand substitutions are expected to bring about DNA ICL formations by the complexes upon visible light irradiation. Also, the photoexcitation of these metal complexes is known to involve ligand to metal based charge transfer processes. cVDC was characterized crystallographically and the crystal structure confirms the *trans*-disposition of the chloride ligands in the complex (Figure 1C). The crystal structure of cVDC shows discrete monomeric vanadium (IV) species with a VO^{2+} moiety bonded to a (4′-phenyl)-2,2′:6′,2″-terpyridine ligand and two chloride ligands (Supplementary Tables S1 and S2, available at *Carcinogenesis* Online). The chloride ligands are positioned *trans* to each other with the Cl (1)-V (1)-Cl (1)′ angle of 165.65°. The terpyridine ligand is bonded through the

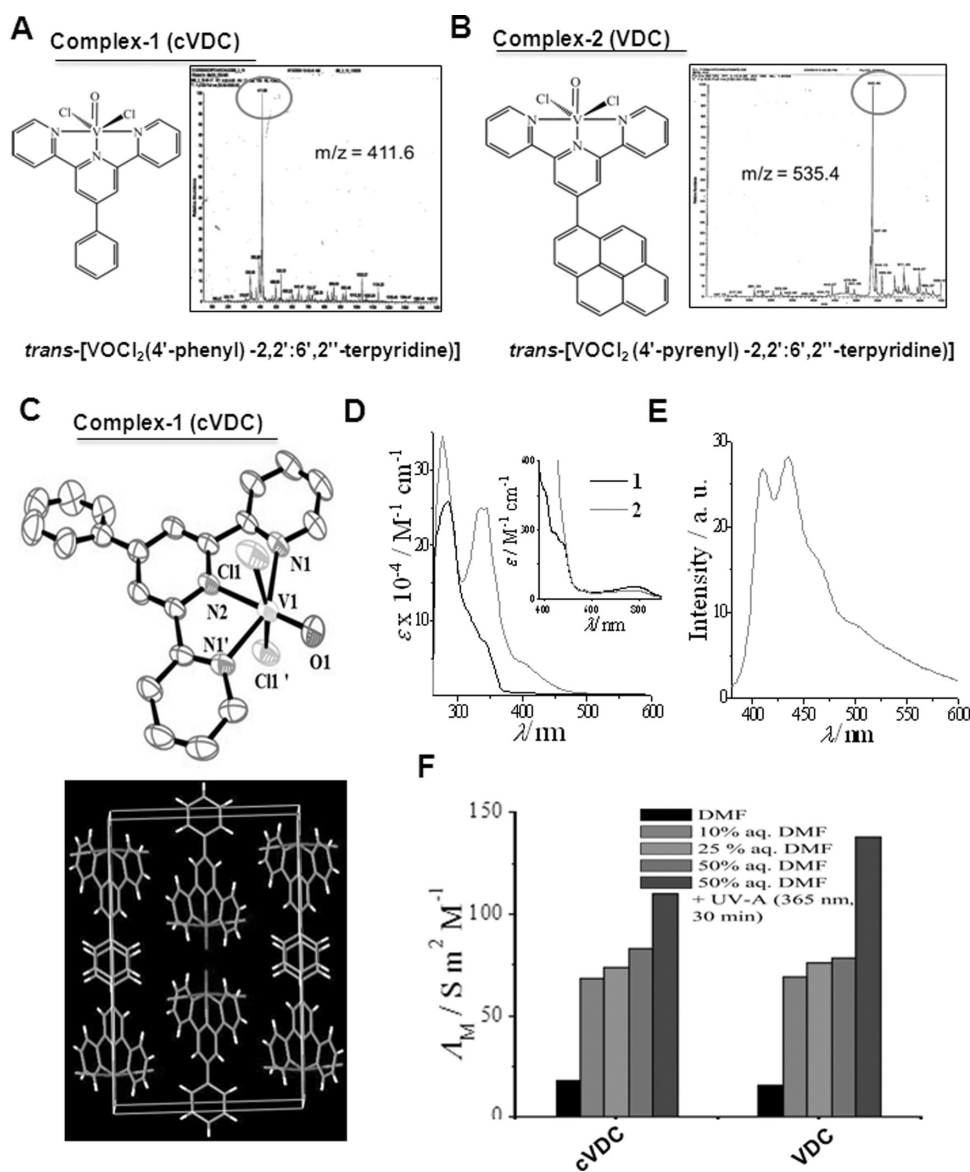**Figure 1.** Design and synthesis of novel photoinducible ICL agent. Chemical structure and ESI-MS spectra of cVDC (**A**) and VDC (**B**) VO2+ complexes. (**C**) An ORTEP view of [VO(Phtpy)Cl₂] (cVDC) showing the atom labeling scheme and 50% probability thermal ellipsoids with unit cell packing diagram. (**D**) Electronic spectra of the ternary oxovanadium (IV) complexes [VO(Phtpy)Cl₂] (cVDC) and [VO(Pytpy)Cl₂] (VDC) in DMF. The inset shows the d–d band in the visible region. (**E**) Emission spectra of VDC in DMSO. (**F**) Changes in conductivity of cVDC and VDC under different conditions.

nitrogen atoms of the pyridyl groups with the V (1)-N (2) distance being ~0.05 Å longer than the terminal V (1)-N (1) and V (1)-N (1)′ distances. The cVDC has a $V^{IV}N_3Cl_2O$ coordination geometry. The V = O distance is ~1.6 Å. The terpyridine ligand displays a meridional mode of binding to the metal center. The structure deviates from an ideal octahedral geometry where the N (1)-V (1)-N (1)′ angle is 146.62 (14)°. Also, the Cl (1)-V (1)-Cl (1)′ angle shows ~14° deviation from the ideal *trans*-disposition. There are four molecules per unit cell as seen in the unit cell packing diagram (Figure 1C). Oxovanadium (IV) complexes *trans*-[VOCl₂(R-tpy)] (1 and 2), where R-tpy is (4′-phenyl)-2,2′:6′,2″-terpyridine (ph-tpy in 1), (4′-pyrenyl)-2,2′:6′,2″-terpyridine (py-tpy in 2), were synthesized in good yield (~75%) from a reaction of the terpyridine liands with vanadium(III) chloride in methanol. The major mass peak observed in the ESI-MS spectra is assignable to the [M–Cl⁻]⁺ species for both the ICL complexes 1 and 2 (Figure 1A and B). The IR spectra of the complexes showed the characteristic infrared bands of ṽ (V=O) at ~970 cm⁻¹ (Supplementary Figure 1A and B, available at *Carcinogenesis* Online). The magnetic moment value of ~1.6 μ_B at 25°C indicates the presence of one-electron paramagnetic 3d¹-V(IV) in the complexes. The electronic absorption spectra of the oxovanadium (IV) complexes in dry DMF show two low-energy low-intensity metal-centered transitions near 810 and 760 nm (Figure 1D and E). A low intensity band observed at 570 nm for the pytpy VDC could be due to ligand-to-metal charge-transfer transition. The remaining bands appearing in the UV-region are assignable to the intraligand π → π* and n → π* transitions. The complexes are stable and highly soluble in DMF, DMSO and MeCN; moderately soluble in water, methanol and ethanol; and poorly soluble in hydrocarbons and chlorinated solvents. The complexes do not show any oxidative response indicating stability of the complexes towards oxidizing agents. cVDC and VDC display an irreversible voltammetric response at –0.56 and –0.83V, respectively, versus S.C.E (Supplementary

Figure 2A and B, available at *Carcinogenesis* Online). This redox process is assignable to the V(IV)/V(III) couple. The complexes are nonelectrolytic in nature and gave molar conductance values of ~15 S m^2/M^1 in dry DMF at 25°C (Figure 1F and Supplementary Figure 3A and B, available at *Carcinogenesis* Online). The complexes were 1:1 electrolyte when the solutions were prepared in 10% aqueous DMF giving molar conductance values of ~70 S m^2/M^1 and the conductivity further increased upon UV-A light (365 nm) irradiation (Figure 1F and Supplementary Figure 3C and D, available at *Carcinogenesis* Online). The observations from ESI-MS, UV-Vis experiments and conductivity data indicate the loss of one of the chloride ligands in polar medium and the loss of the other chloride upon UV-A light irradiation.

Generation of DNA monoadducts by VDC

NER is a functionally conserved pathway from bacteria to human cells to repair lesions generated in the form of DNA monoadducts and DNA protein crosslinks (3). In *E. coli*, UvrD helicase is known to participate in NER (32), and loss of *uvrD* compromises

monoadduct repair resulting in extreme sensitivity to DNA damaging agents such as methyl methane sulfonate (32). It has been shown that UvrD is essential for the replication of plasmid DNAs containing varied DNA lesions (33). To validate the formation of monoadduct by VDC, we incubated supercoiled pUC19 with mock (DMSO), cVDC and VDC in dark (Figure 2A). The DNA was purified and equal amount of mock-treated/treated DNA was used to transform *SMR6319* WT and Δ*uvrD E. coli* strains, which were then grown under ampicillin selection. The number of ampicillin resistant colonies in cells transformed with cVDC/VDC treated DNA relative to the number of colonies in mock treated DNA was taken as a measure of plasmid replication (Supplementary Figure 4A, available at *Carcinogenesis* Online). It was observed that in contrast to the WT cells, Δ*uvrD* cells showed a drastic reduction (~8-fold) in ampicillin resistant colonies with cVDC/VDC damaged plasmid compared to WT cells (Figure 2A). The potency of cVDC and VDC to generate DNA monoadducts *in vivo* was studied by analysing the survival of WT and Δ*uvrD* cells when treated with cVDC/VDC in dark. In agreement with the repair of *in vitro* formed monoadducts in dark, treatment of
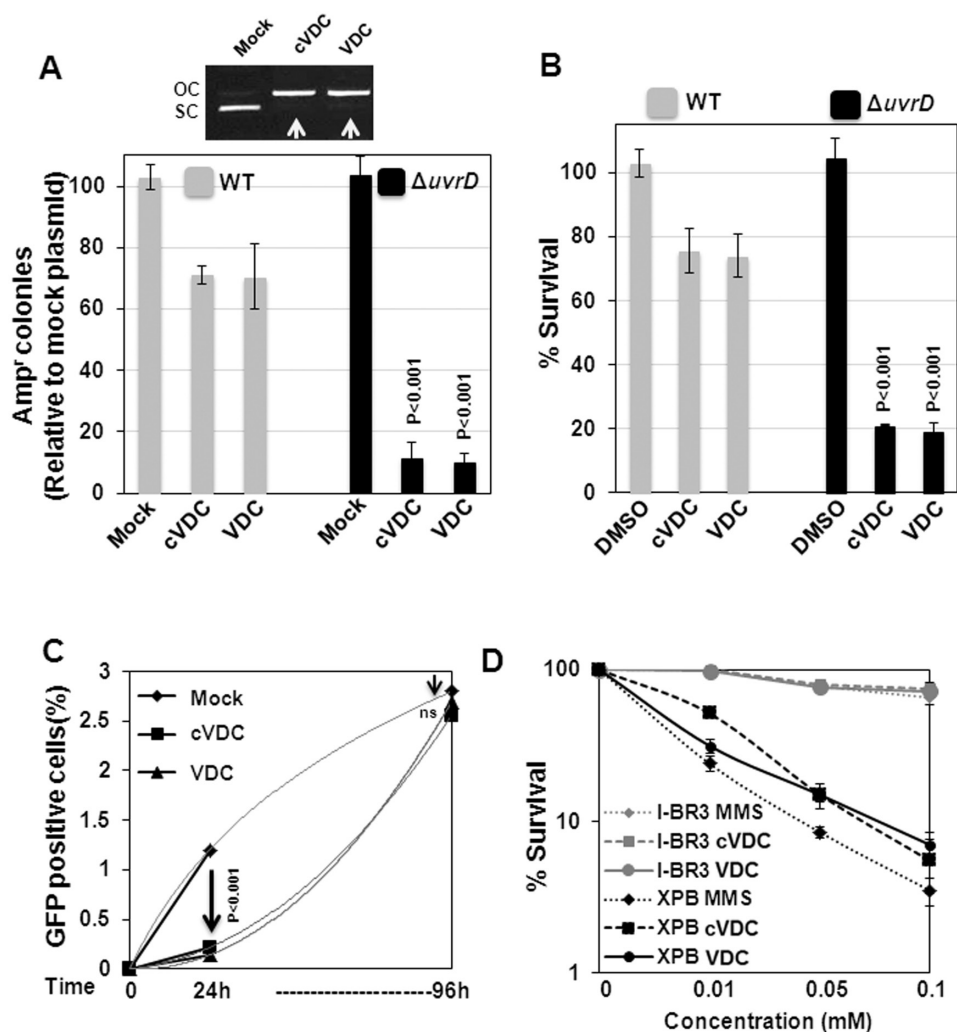

Figure 2. cVDC and VDC induce monoadducts in DNA *in vitro* and *ex vivo*. (**A**) Representative gel picture for cVDC and VDC treated pUC19 plasmid DNA (top panel). SC: Supercoiled; OC: Open circular. Ampicillin resistant (Amp^r) colonies of WT and Δ*uvrD E. coli* cells transformed with mock/cVDC/VDC treated pUC19 plasmid DNA. The experimental points represent mean ± standard deviations of three independent experiments. (**B**) Survival of WT and Δ*uvrD E. coli* cells after exposure to cVDC and VDC. WT or Δ*uvrD E. coli* cells were treated with mock (DMSO), cVDC or VDC (as described in Materials and Methods) and colony formation was monitored after 12 h of incubation. The experimental points represent mean ± standard deviations of three independent experiments. (**C**) Quantification of GFP positive cells as a measure of adduct repair at various time points. (**D**) Cell survival of IBR3 and XPB cells after treatment with indicated concentrations of cVDC and VDC in dark.

Δ*uvrD* cells with cVDC/VDC led to a dramatic reduction in cell survival (~4-fold) compared to WT cells (Figure 2B). These data suggest that cVDC and VDC form monoadducts.

To validate the above findings in mammalian system, we incubated pcDNA3βeGFP plasmid with cVDC and VDC in dark to allow formation of monoadducts in the DNA (Supplementary Figure 5, available at *Carcinogenesis* Online). The purified plasmid was used to transfect HEK293T cells which support replication of ectopic plasmids owing to the presence of large T-antigen. Supplementary Figure 4B, available at *Carcinogenesis* Online, shows the schematic diagram of the assay. As can be seen with data in Figure 2C, at 24 h, we observed low levels of GFP expression in damaged plasmid as compared to mock treated plasmid, likely due to incomplete repair of the damaged plasmid. However, in the later time, repair allows faithful replication and maintenance of the plasmid DNA over several generations. As a result, at 96 h, levels of GFP expression in cells transfected with damaged DNA matched that of the untreated DNA (Figure 2C and Supplementary Figure 5, available at *Carcinogenesis* Online), suggesting the complete repair and replication of damaged plasmid DNA. These results suggest that both cVDC and VDC form stable DNA monoadducts in dark.

To further understand the *in vivo* generation of DNA monoadducts by cVDC and VDC in mammalian system, firstly cellular incorporation of VDC was assessed by flowcytometry. Our results from various cell lines revealed ~95% incorporation by 6 h post-treatment (Supplementary Figure 6A and B, available at *Carcinogenesis* Online). Microscopic examination showed presence of VDC in both cytoplasm and nucleus (Supplementary Figure 6C, available at *Carcinogenesis* Online). In these experiments, cVDC couldn't be identified owing to its lack of fluorescence. Further, we tested the retention of VDC on the chromosome by assessing the vanadium in the whole cell and chromatin fraction. Interestingly, ~50% of vanadium was detected in the chromatin fraction in dark (Supplementary Figure 7A–C, available at *Carcinogenesis* Online), suggesting that VDC forms monoadduct with DNA in dark (Supplementary Figure 7D, available at *Carcinogenesis* Online). To validate monoadduct formation by VDC in mammalian cells, we tested the cell survival of NER deficient XPB cells in comparison with WT IBR3 fibroblast cells. Notably, XPB cells exhibited high degree of sensitivity to both cVDC and VDC in dark along with methyl methane sulfonate as a positive control (Figure 2D). Together, these data suggest that cVDC/VDC can form monoadducts in dark *in vitro* and *ex vivo*.

VDC induces DNA crosslinks *in vitro* and *ex vivo*

cVDC and VDC complexes were later tested for potential crosslinking ability using linearized pUC19 plasmid DNA in alkaline electrophoresis assay, which is specifically sensitive to the presence of inter-strand crosslinks in DNA. cVDC failed to crosslink the linearized DNA molecules (Supplementary Figure 8A, available at *Carcinogenesis* Online), whereas exposure of VDC with UV-A or visible light resulted in an efficient crosslinked DNA (Figure 3A). To study DNA crosslink formation in the cell, we performed modified comet assay (34) to measure the extent of genome wide crosslinks using conventional crosslinking agents such as MMC and Melphalan. Tail moment, a measure of relative electrophoretic mobility, decreased with increasing concentrations of MMC and Melphalan for 2 h in HeLa cells (Supplementary Figure 8B and C, available at *Carcinogenesis* Online). Our data with *in vitro* DNA crosslink formation by VDC was substantiated by alkaline comet assay, where it was observed that cVDC failed to form DNA crosslinks (Figure 3C),

whereas VDC formed efficient DNA ICLs upon UV-A and visible light irradiation compared to dark (Figure 3B and D). Together, these results suggest that while both cVDC and VDC are able to form DNA monoadducts to similar extent in the dark, only VDC engages in the formation of DNA crosslinks upon photo-activation by UV/Visible light.

Progressive restoration of tail moment after DNA crosslink induction can serve as a marker for ICL repair through crosslink unhooking and double strand break (DSB) generation. Indeed, we observed a gradual restoration of tail moment after DNA crosslink induction by various ICL agents including VDC upon recovery (Figure 3E). The kinetics of repair of UV-A or visible light activated VDC-induced DNA crosslink was comparable with those generated by MMC or Melphalan (Figure 3E), suggesting the reversible nature of crosslinks induced by VDC.

VDC induces FA pathway of ICL repair

Formation of inter-strand crosslinks perturbs the cellular processes of DNA replication and transcription (5). Here, we measured the extent of DNA replication by BrdU incorporation in VDC treated cells under dark/UV-A/visible conditions. We observed a significant suppression of DNA synthesis in VDC treated cells in dark (Figure 4A). In a stark contrast, DNA replication was completely abrogated in VDC treated cells under UV-A or visible light (Figure 4A). Cellular ICLs are recognized and processed by crosslink repair machinery including FA pathway proteins (35). Hence, we examined whether VDC can elicit FA pathway response by analyzing the FANCD2 focus formation. Strikingly, similar to MMC, VDC induced >4-fold increase in FANCD2 nuclear foci after irradiation with visible light (Figure 4B). The FA pathway activation by VDC after visible light irradiation was further confirmed by examining the FANCD2 monoubiquitination (Figure 4C). The extent of DSBs generated after processing of VDC induced crosslinks was measured by H2AX S139 phosphorylation (γH2AX) (Figure 4D). RAD51 protein plays key role in the repair of DSBs by HR (17,36,37). Notably, VDC treated cells exhibited discrete RAD51 nuclear foci formation and chromatin loading (Supplementary Figure 9A and B, Figure 4E). Furthermore, the reversible nature of the crosslink generated by VDC was studied by recovering cells after crosslink induction. DSB markers such as γH2AX and XRCC3 phosphorylation at S225 (28) along with RAD51 foci were monitored across recovery time points (Figure 4F and Supplementary Figure 9C, available at *Carcinogenesis* Online). As expected, DSB generation and RAD51 foci formation peaked at early time points of recovery, and showed progressive decline with time, with full recovery at 12–15 h (Figure 4F and Supplementary Figure 9C, available at *Carcinogenesis* Online).

VDC exerts cellular hypersensitivity in the FA pathway and HR deficient cells

To further understand the potency of VDC after photoinduction, we examined the cell survival of various cancer as well as normal cells after incubation with different doses of VDC. Compared to dark, photoinduction of VDC by UV-A and visible light caused several fold reduction in cell survival of HeLa, MCF-7 and U2OS cancer cells as well as normal IBR3 cells (Figure 5A). VDC induced sensitivity in these cells was observed at higher doses (1–10 μM). A recent report as well as our group identified that RAD51C is a new player in the FA pathway of ICL repair (29,38). Hence, we examined the sensitivity of cells following depletion of RAD51C and various other FA pathway proteins such as FANCM and FANCJ in HeLa cells. Interestingly, depletion of these
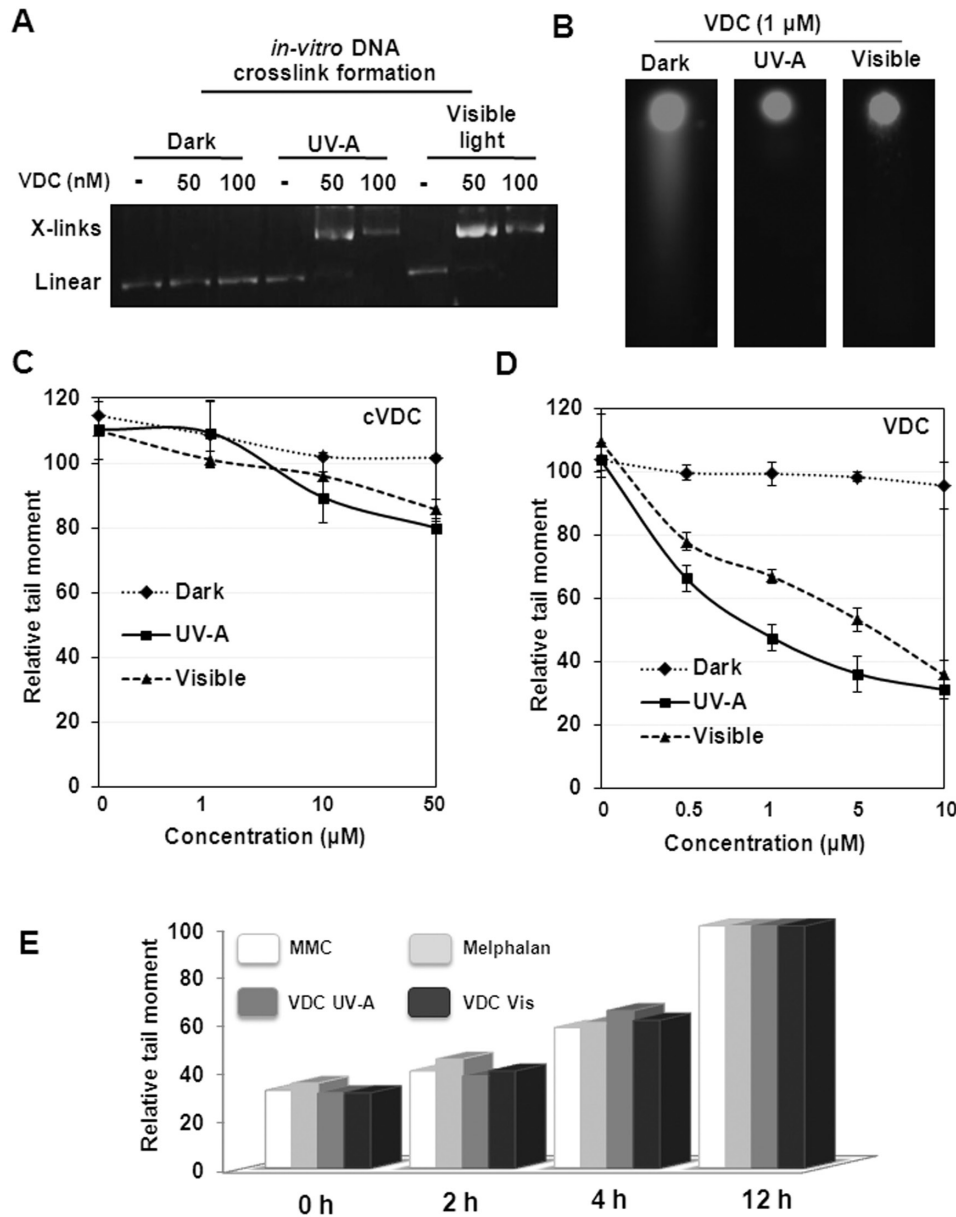
Figure 3. VDC induces DNA crosslinks *in vitro* and *ex vivo* upon photoactivation. (**A**) VDC induces DNA crosslinks *in vitro* in a plasmid based assay. Formation of DNA crosslink was examined using linearized pUC19 plasmid. The DNA was resolved by alkaline agarose gel electrophoresis and visualized by ethidium bromide staining. (**B**) Representative images of alkaline comet assay from the HeLa cells treated with VDC (1 μM, 6 h) in dark or after exposure to UV-A and visible light. Dose-dependent decrease in relative tail moment in HeLa cells after photoinduction of cVDC (**C**) and VDC (**D**) compared to dark. (**E**) Time-dependent restoration of relative tail moment in HeLa cells following treatment with indicated ICL-inducing agents.

FA proteins resulted in great degree of sensitivity to VDC in the nanomolar concentration, and this sensitivity was evident only after photoinduction by UV-A and visible light (Figure 5B and Supplementary Figure 10A, available at *Carcinogenesis* Online). Further, we examined the sensitivity of RAD51C deficient CL-V4B hamster cells to VDC. Incubation of CL-V4B cells with increasing doses of VDC coupled with UV-A and visible light irradiation resulted in >10-fold reduction in cell survival when compared with parental WT V79B cells (Supplementary Figure 11A and 10B, available at *Carcinogenesis* Online). In response to unrepaired ICLs, activated cell cycle checkpoints arrest the cells in G2/M (29). Indeed, progression of CL-V4B cells through S and G2 phases was affected after VDC induced crosslinks and led to a prolonged accumulation in G2/M (Supplementary Figure 11B,

available at *Carcinogenesis* Online). However, parental V79B cells recovered from ICL induced stress and resumed normal cell cycle progression (Supplementary Figure 11B, available at *Carcinogenesis* Online). The ICL repair kinetics can be studied by following the CHK1 S345 phosphorylation status (39). After VDC induced crosslink DNA damage, CHK1 S345 phosphorylation was evident by 4h and this phosphorylation diminishes by 24h, indicating the completion of ICL repair in WT cells (Figure 5C and D). Notably, CHK1 activation was extended in RAD51C and FANCJ depleted HeLa cells, suggesting the persistence of unrepaired crosslinks generated by VDC (Figure 5C and D). Prolonged checkpoint activation leads to apoptosis and secondary necrosis (40). We tested whether VDC induced cell death in FA pathway defective cells is due to the sustained activation of checkpoint
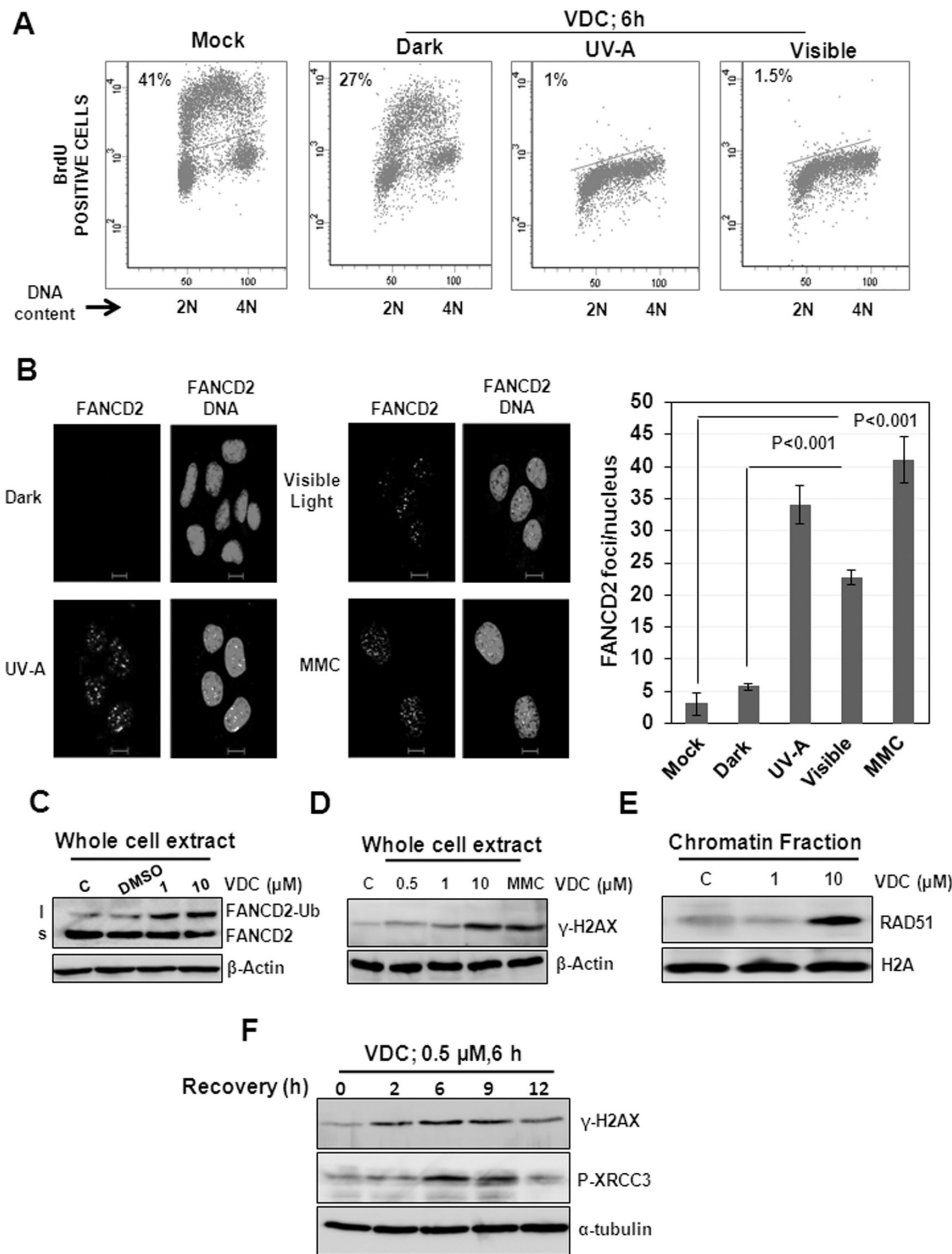
Figure 4. VDC activates FA pathway of ICL repair. (**A**) Incorporation of BrdU as a measure of replication/proliferation of HeLa cells after treatment of cells with VDC. (**B**) Analysis of FANCND2 foci in HeLa cells after DNA crosslink formation by VDC and MMC. Scale bar, 10 μm. Bar graph represents mean ± SD from three independent experiments. *P* value is obtained in comparison with mock treatment in the case of MMC, and dark for VDC activation after UV-A and visible light. (**C**) Analysis of FANCD2 monoubiquitination after VDC activation under visible light. (**D**) Analysis of γ-H2AX after VDC activation under visible light in HeLa cells. (**E**) Analysis of chromatin-bound RAD51 after ICL2 induction by visible light. Histone H2A was used as a chromatin marker. (**F**) Analysis of DSB markers γ-H2AX and p-XRCC3 S225 at indicated recovery time points after treatment with VDC.

after DNA crosslink induction. Our analysis with annexin-V and propidium iodide analysis after 15 h of crosslink induction revealed that RAD51C depleted cells showed remarkable levels of cell death due to apoptosis (Supplementary Figure 12, available at *Carcinogenesis* Online).

Germline mutations in *RAD51C* confer susceptibility to VDC induced crosslinks

RAD51C G125V and L138F pathological mutants were identified in breast and ovarian cancers with reported loss of heterozygosity in tumor cells (41,42). These mutations in RAD51C lead to

loss of HR and DNA damage response functions (29). In addition, RAD51C L138F exhibit defect in fork stability and replication restart (31). PolyADP ribose polymerases (PARP) inhibitors are used to specifically target HR defective tumor cells with great success (43). We recently reported that cells expressing RAD51C pathological mutants can be specifically targeted by using PARP inhibitors (44). To test whether VDC can be used to sensitize HR defective cancer cells with further advantage of controlled activation, we treated cells stably expressing RAD51C G125V and L138F pathological mutants with increasing doses of VDC and upon photoinduction, cell survival was measured. Interestingly,
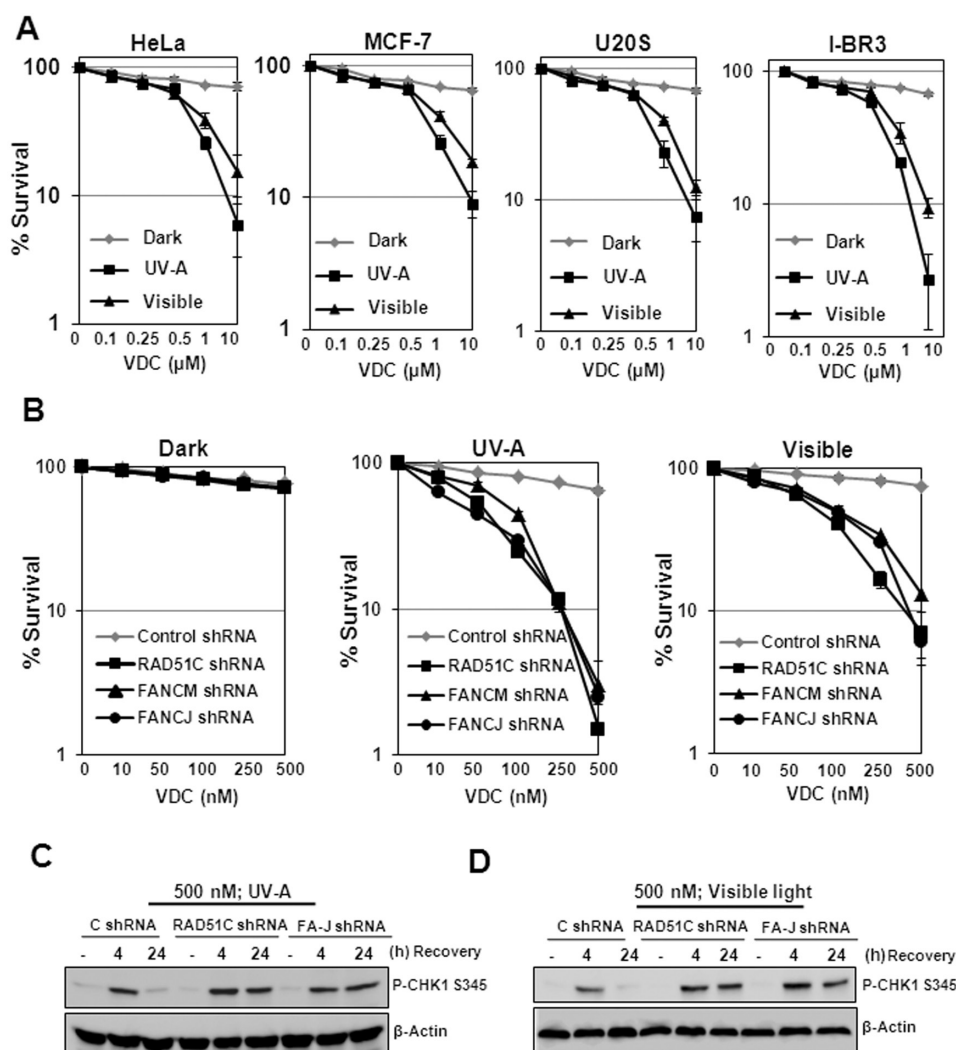
Figure 5. VDC induces cytotoxicity in normal and cancer cells. FA pathway defective cells show hypersensitivity to VDC after photoinduction. (**A**) Sensitivity of various human cancerous HeLa, MCF7 and U2OS cells and normal IBR3 cells to VDC in dark or after activation by UV-A and visible light. (**B**) Sensitivity of HeLa cells after depletion of FA pathway proteins FANCO (RAD51C), FANCM and FANCJ compared to control cells to indicated concentration of VDC in dark or after activation by UV-A and visible light. (**C**) CHK1 phosphorylation after VDC activation by UV-A and visible light (**D**) at indicated recovery time points in RAD51C and FANCJ depleted cells compared to control cells.

compared to control WT RAD51C expressing cells, RAD51C pathological mutants exhibited significant reduction (~10-fold) in cell survival (Figure 6A). Together these data suggest that VDC is a novel photoinducible crosslinking agent which can be used for cancer therapy.

Discussion

The ICL-based chemotherapy is still in a stage of infancy due to its cytotoxicity and variety of side effects towards normal cells (19). Photoactivable crosslinking agents are emerging as an effective solution to this problem, which prevent the need for high doses and constitutive generation of ICLs during the period of therapy. Moreover, usage of photoactivable crosslinking agents renders non-cancer cells with reversible side effects and allows patients to tolerate prolonged treatment (20), thus maximizing the success of treatment regime. However, currently Psoralen is the only photoinducible crosslinking agent used for clinical application in cancer therapy (5,8). Psoralen consists of a furan ring fused to a coumarin. The planar tricycle intercalates

into duplex DNA and upon absorption of a quantum of light, the 4,5-furan double bond undergoes photocycloaddition to the 5,6-double bond of a thymidine, leading to a monoadduct. Absorption of a second quantum of light by coumarin leads to cyclization with the 5,6-double bond of the adjacent pyrimidine, thus generating a crosslink (8). However, the peak absorption of Psoralen is at ~300 nm, limiting its activation only in the UV-A range (19), which can induce skin cancer in patients under therapy. Owing to the major clinical limitation of Psoralen that it can be activated only by UV-A radiation which can induce skin cancer (19), we have developed a novel photoinducible crosslinking agent (VDC) which can be activated in visible light. Moreover, due to its intrinsic fluorescence, the cellular uptake of VDC also can be examined.

Germline mutations in HR pathway genes such as *BRCA1*, *BRCA2* and *RAD51C* cause hereditary breast and ovarian cancers (45). Since HR is a major DSB repair pathway (46,47), induction of more DSBs through ICLs is a potential strategy to specifically target HR deficient cancer cells. In this direction, the newly identified photoinducible VDC complex could serve as a potential
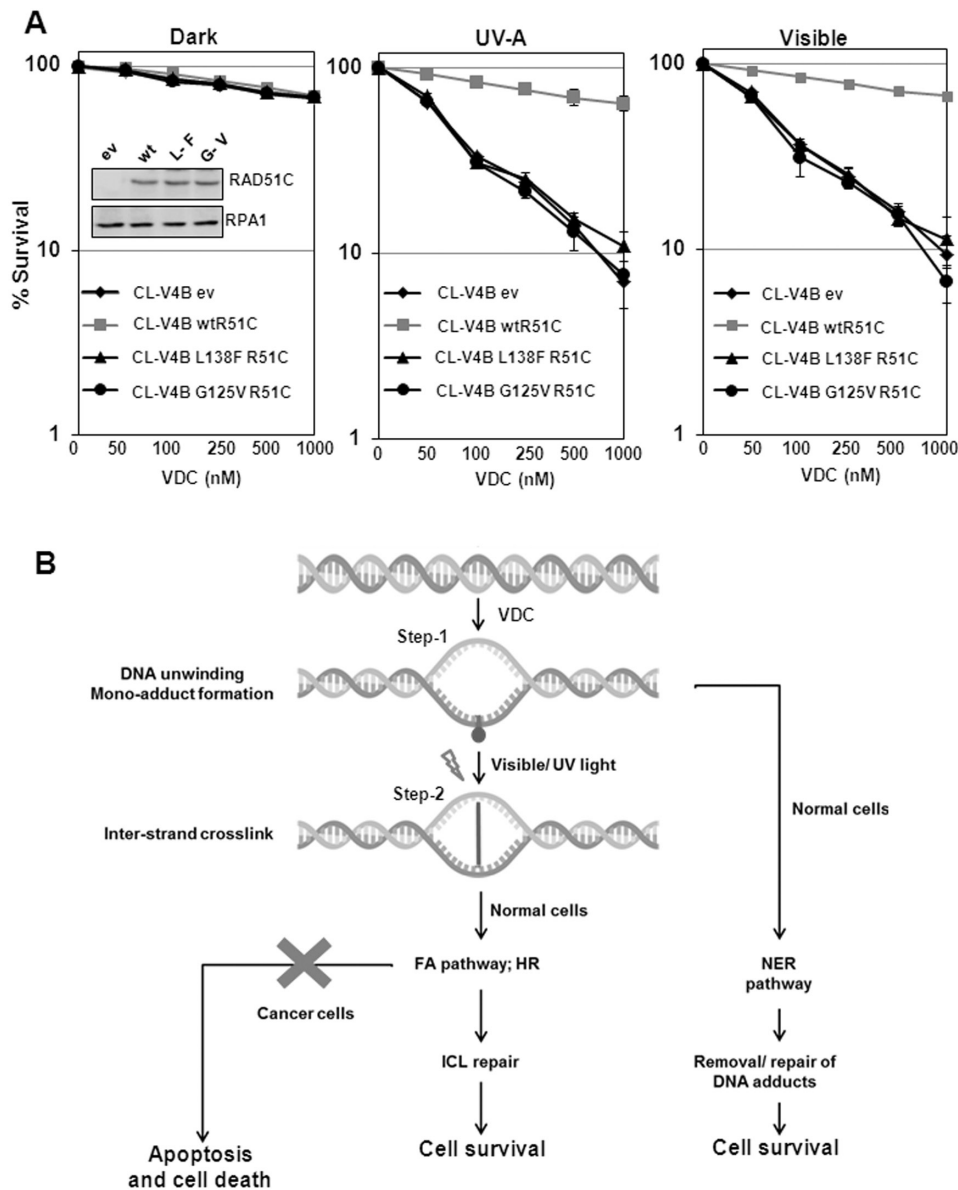
Figure 6. VDC is a novel photoinducible ICL agent for targeting FA and HR pathway defective cells. (**A**) Sensitivity of CL-V4B cells stably expressing RAD51C pathological mutants G125V and L138F mutants compared to WT cells to indicated concentration of VDC in dark or after photoactivation by UV-A and visible light. Expression of WT and mutant RAD51C proteins are shown in inside panel. RPA1 was taken as loading control. (**B**) Model for the mechanism of action of VDC induced toxicity and its therapeutic potential to sensitize tumors with defects in FA/HR pathway. VDC binds to DNA and forms a monoadduct in dark. Irradiation of the tumorous tissue with visible light leads to formation of an ICL in the DNA. In the non-tumorous cells, NER carries out robust repair of the monoadducts, thus preventing any off-target effects. In normal cells, ICL generation leads to activation of the FA pathway, followed by HR, which effectively repairs the ICLs leading to cell survival. In contrast, cancer cells harboring mutations in FA/HR pathway genes like *RAD51C*, *BRCA1/2*, *FANCJ* are driven towards apoptosis and cell death.

drug for targeted tumor therapy of patients with mutations in HR pathway with limited/no side effects upon induction by visible light.

Our analysis of core vanadium detection with whole cell extract and chromatin fraction revealed that a significant fraction (~50%) of VDC was retained on the chromatin in dark, suggesting that VDC forms a stable oxovanadium (IV) complex with DNA. We anticipated that VDC may be forming a monoadduct with DNA in dark. Indeed, our plasmid-based *in vivo* studies revealed that the relative colony-forming ability of NER defective *E. coli* Δ*uvrD* strain was severely diminished after transformation with VDC treated plasmids. In addition, *E. coli* Δ*uvrD* and NER deficient human *XPB* cells, defective in DNA monoadduct repair, exhibited hypersensitivity to VDC, indicating that VDC potentially forms monoadduct with DNA *in vitro* as well as *ex vivo*. This was further corroborated by low levels of GFP expression with VDC treated eGFP plasmid in human HEK293T cells. Interestingly, the expression levels were restored at later time points, indicating the progressive repair of adducts on plasmid DNA. VDC underwent loss of one of the chloride ligands in polar medium and strikingly, irradiation with UV-A led to the loss of the second chloride, indicating that photoinduction of VDC may result in the formation of ICLs. Indeed, our observations with *in vitro* plasmid-based and alkaline comet assay showed that VDC forms DNA crosslinks after activation under UV light. VDC exhibited maximum absorption in the range of 760–810 nm, which

prompted us to test the ability of VDC to form DNA crosslinks in visible light. Strikingly, our data with alkaline comet experiments showed that VDC was equally potent at forming DNA crosslinks after activation with UV-A or visible light. Moreover, crosslink formation by VDC upon irradiation in the visible range was comparable to that of known potent ICL agents such as MMC and melphalan. Photoactivation of the molecule under UV light irradiation is probably associated with the intraligand $\pi \to \pi^*$ and $n \to \pi^*$ transitions of the molecule. The ligand centered π-electrons get excited upon UV light irradiation and when these electrons return to their ground states, the energy released facilitates the release of the chloro ligands, thus creating vacant site at the metal center for binding to the DNA bases. The visible light induced photoactivation of VDC could be due to the synergistic involvement of low-energy low-intensity metal-centered transitions near 810 nm and ligand-to-metal charge-transfer transition at 570 nm. The main role is possibly played by the ligand-to-metal charge-transfer transition at 570 nm which, when the molecule is excited, facilitates the transfer of charge from the π-electron rich pyrenyl terpyridine ligand to the metal center which in turn helps the release of the chloro ligand and thus creating a site for the DNA bases to bind to the vanadium metal. Exposure to VDC led to FANCD2 focus formation and monoubiquitination, thus further confirming the generation of DNA crosslinks *ex vivo*. This was further supported by the generation of γ-H2AX and enhanced recruitment of RAD51 to the chromatin following treatment with VDC. Additionally, VDC was found to be highly potent in inhibiting replication as observed in the BrdU incorporation assay.

Our studies with cell survival/cytotoxic assays clearly show that VDC does not induce sensitivity in dark, owing to the robust repair of monoadducts in normal cells (Figure 6B). However, photoinduction of VDC with UV or visible light resulted in hypersensitivity (8–10-fold) at μM concentrations, suggesting that photoactivated VDC is a potent cytotoxic agent. Interestingly, cells depleted of FA pathway proteins such as RAD51C, FANCM and FANCJ exhibited heightened sensitivity (>10-fold) compared to control cells at nM concentrations of VDC, indicating that VDC can indeed be used for targeted cancer therapy with minimal side-effects to normal cells. In corroboration with these results, we found that VDC exerted checkpoint response in normal cells and this activation remained persistent in RAD51C and FANCJ depleted cells, owing to the lack of repair of generated DSBs. Also, this prolonged DNA damage drove the cells towards death, as seen by elevated levels of apoptosis in RAD51C depleted cells. Taken together, these observations imply that VDC can be considered as an effective anticancer agent (Figure 6B).

FA patients develop many types of cancers including myeloid leukemia and head and neck cancers (45,48,49). Notably, our data clearly shows that low doses of VDC are highly effective in inducing cell death in FA pathway deficient cells, implying that VDC can be an effective drug for the treatment of cancers associated with FA patients. Familial breast and ovarian cancers as well as prostate cancers arise due to germline mutations in *BRCA1*, *BRCA2*, *PALB2* and *FANCJ* which are known to regulate ICL and DSB repair by HR (17,45). Recently, *RAD51C* missense mutations have been identified in breast and ovarian cancers (41,42) and our previous study shows that these pathological mutants are defective for HR-mediated DSB repair (29). Interestingly, we find that cells expressing RAD51C missense mutants are hypersensitive to VDC upon irradiation with UV and visible light. These data suggest that cancer cells arising due to missense mutations in DNA repair genes can be specifically targeted by VDC.

In summary, VDC is a novel photoinducible ICL agent which can be activated in visible light (Figure 6B). Due to the intrinsic fluorescence property of VDC, its bioavailability and stability can be conveniently monitored at the target site. The photoactivatable VDC complex thus presents a new direction in cancer chemotherapy where the compound is non-toxic in dark and its activity can be selectively induced by visible light (Figure 6B). This strategy provides a better methodology than photodynamic therapy (PDT) in which the activity of a PDT drug is dependent on several factors including high yield of singlet oxygen generation. Additionally, the porphyrin-based PDT drugs show severe skin sensitivity and hepatotoxicity (50). Light activated ICL generation thus overcomes the drawbacks of the conventional PDT agents. As VDC can be activated with visible light, we speculate that it is an ideal drug candidate for cancer treatment to a wide range of cancer cells. Moreover, we propose that VDC can be used as an anticancer drug in FA-BRCA pathway defective patients (Figure 6B). Finally, with the rapid advances in our understanding of ICL repair, we anticipate that small molecule inhibitors targeted towards FA-BRCA pathway will be identified in future, that could further improve the clinical effectiveness of VDC by combinatorial therapy. However, further studies including animal model is required to understand the efficacy of VDC for clinical application of cancer treatment.

Supplementary material

Supplementary Figures 1–12 can be found at http://carcin.oxfordjournals.org/

Funding

Acknowledgements

References

1. Jackson, S.P. et al. (2009) The DNA-damage response in human biology and disease. Nature, 461, 1071–1078.
2. Shiloh, Y. et al. (2013) The ATM protein kinase: regulating the cellular response to genotoxic stress, and more. Nat. Rev. Mol. Cell Biol., 14, 197–210.
3. Hoeijmakers, J.H. (2001) Genome maintenance mechanisms for preventing cancer. Nature, 411, 366–374.
4. Torgovnick, A. et al. (2015) DNA repair mechanisms in cancer development and therapy. Front. Genet., 6, 157.
5. Deans, A.J. et al. (2011) DNA interstrand crosslink repair and cancer. Nat. Rev. Cancer, 11, 467–480.

6. Kee, Y. et al. (2010) Expanded roles of the Fanconi anemia pathway in preserving genomic stability. Genes Dev., 24, 1680–1694.
7. Noll, D.M. et al. (2006) Formation and repair of interstrand cross-links in DNA. Chem. Rev., 106, 277–301.
8. Rajski, S.R. et al. (1998) DNA cross-linking agents as antitumor drugs. Chem. Rev., 98, 2723–2796.
9. Momtaz, K. et al. (1998) The benefits and risks of long-term PUVA photochemotherapy. Dermatol. Clin., 16, 227–234.
10. Shiloh, Y. (2014) ATM: expanding roles as a chief guardian of genome stability. Exp. Cell Res., 329, 154–161.
11. Jeggo, P.A. et al. (2006) Contribution of DNA repair and cell cycle checkpoint arrest to the maintenance of genomic stability. DNA Repair (Amst). 5, 1192–1198.
12. Bartek, J. et al. (2004) Checking on DNA damage in S phase. Nat. Rev. Mol. Cell Biol., 5, 792–804.
13. D'Andrea, A.D. (2001) Cellular function of the Fanconi anemia pathway. Nat. Med., 7, 1259–1260.
14. Kee, Y. et al. (2012) Molecular pathogenesis and clinical management of Fanconi anemia. J. Clin. Invest., 122, 3799–3806.
15. Clauson, C. et al. (2013) Advances in understanding the complex mechanisms of DNA interstrand cross-link repair. Cold Spring Harb. Perspect. Biol., 5, a012732.
16. Duxin, J.P. et al. (2015) What is the DNA repair defect underlying Fanconi anemia? Curr. Opin. Cell Biol., 37, 49–60.
17. Somyajit, K. et al. (2010) RAD51C: a novel cancer susceptibility gene is linked to Fanconi anemia and breast cancer. Carcinogenesis, 31, 2031–2038.
18. Walden, H. et al. (2014) The Fanconi anemia DNA repair pathway: structural and functional insights into a complex disorder. Annu. Rev. Biophys., 43, 257–278.
19. Rabik, C.A. et al. (2007) Molecular mechanisms of resistance and toxicity associated with platinating agents. Cancer Treat. Rev., 33, 9–23.
20. Huang, Y. et al. (2013) DNA crosslinking damage and cancer - a tale of friend and foe. Transl. Cancer Res., 2, 144–154.
21. Selvakumaran, M. et al. (2003) Enhanced cisplatin cytotoxicity by disturbing the nucleotide excision repair pathway in ovarian cancer cell lines. Cancer Res., 63, 1311–1316.
22. Taniguchi, T. et al. (2003) Disruption of the Fanconi anemia-BRCA pathway in cisplatin-sensitive ovarian tumors. Nat. Med., 9, 568–574.
23. Mackay, F.S. et al. (2007) A potent cytotoxic photoactivated platinum complex. Proc. Natl. Acad. Sci. USA, 104, 20743–20748.
24. Heringova, P. et al. (2006) Transplatin is cytotoxic when photoactivated: enhanced formation of DNA cross-links. J. Med. Chem., 49, 7792–7798.
25. Wang, P. et al. (2003) A potent, water-soluble and photoinducible DNA cross-linking agent. J. Am. Chem. Soc., 125, 1116–1117.
26. Banik, B. et al. (2014) Carbohydrate-appended photocytotoxic (imidazophenanthroline)-oxovanadium(IV) complexes for cellular targeting and imaging. Dalton Trans., 43, 1321–1331.
27. Rabik, C.A. et al. (2007) Molecular mechanisms of resistance and toxicity associated with platinating agents. Cancer Treat. Rev., 33, 9–23.
28. Somyajit, K. et al. (2013) ATM- and ATR-mediated phosphorylation of XRCC3 regulates DNA double-strand break-induced checkpoint activation and repair. Mol. Cell. Biol., 33, 1830–1844.
29. Somyajit, K. et al. (2012) Distinct roles of FANCO/RAD51C protein in DNA damage signaling and repair: implications for Fanconi anemia and breast cancer susceptibility. J. Biol. Chem., 287, 3366–3380

30. Godthelp, B.C. et al. (2002) Mammalian Rad51C contributes to DNA cross-link resistance, sister chromatid cohesion and genomic stability. Nucleic Acids Res., 30, 2172–2182.
31. Somyajit, K. et al. (2015) Mammalian RAD51 paralogs protect nascent DNA at stalled forks and mediate replication restart. Nucleic Acids Res., 43, 9835–9855.
32. Kisker, C. et al. (2013) Prokaryotic nucleotide excision repair. Cold Spring Harb. Perspect. Biol., 5, a012591.
33. Kumari, A. et al. (2010) Modulation of UvrD helicase activity by covalent DNA-protein cross-links. J. Biol. Chem., 285, 21313–21322.
34. Rothfuss, A. et al. (2004) Repair kinetics of genomic interstrand DNA cross-links: evidence for DNA double-strand break-dependent activation of the Fanconi anemia/BRCA pathway. Mol. Cell. Biol., 24, 123–134.
35. Kupfer, G.M. (2013) Fanconi anemia: a signal transduction and DNA repair pathway. Yale J. Biol. Med., 86, 491–497.
36. Sung, P. et al. (2006) Mechanism of homologous recombination: mediators and helicases take on regulatory functions. Nat. Rev. Mol. Cell Biol., 7, 739–750.
37. Moynahan, M.E. et al. (2010) Mitotic homologous recombination maintains genomic stability and suppresses tumorigenesis. Nat. Rev. Mol. Cell Biol., 11, 196–207.
38. Vaz, F. et al. (2010) Mutation of the RAD51C gene in a Fanconi anemia-like disorder. Nat. Genet., 42, 406–409.
39. Zeman, M.K. et al. (2014) Causes and consequences of replication stress. Nat. Cell Biol., 16, 2–9.
40. Orth, J.D. et al. (2012) Prolonged mitotic arrest triggers partial activation of apoptosis, resulting in DNA damage and p53 induction. Mol. Biol. Cell, 23, 567–576.
41. Osorio, A. et al. (2012) Predominance of pathogenic missense variants in the RAD51C gene occurring in breast and ovarian cancer families. Hum. Mol. Genet., 21, 2889–2898.
42. Meindl, A. et al. (2010) Germline mutations in breast and ovarian cancer pedigrees establish RAD51C as a human cancer susceptibility gene. Nat. Genet., 42, 410–414.
43. Helleday, T. (2013) Putting poly (ADP-ribose) polymerase and other DNA repair inhibitors into clinical practice. Curr. Opin. Oncol., 25, 609–614.
44. Somyajit, K. et al. (2015) Enhanced non-homologous end joining contributes toward synthetic lethality of pathological RAD51C mutants with poly (ADP-ribose) polymerase. Carcinogenesis, 36, 13–24.
45. D'Andrea, A.D. (2010) Susceptibility pathways in Fanconi's anemia and breast cancer. N. Engl. J. Med., 362, 1909–1919.
46. Hartlerode, A.J. et al. (2009) Mechanisms of double-strand break repair in somatic mammalian cells. Biochem. J., 423, 157–168.
47. Shrivastav, M. et al. (2008) Regulation of DNA double-strand break repair pathway choice. Cell Res., 18, 134–147.
48. Mathew, C.G. (2006) Fanconi anaemia genes and susceptibility to cancer. Oncogene, 25, 5875–5884.
49. Kutler, D.I. et al. (2003) High incidence of head and neck squamous cell carcinoma in patients with Fanconi anemia. Arch. Otolaryngol. Head. Neck Surg., 129, 106–112.
50. Huang, Z. (2005) A review of progress in clinical photodynamic therapy. Technol. Cancer Res. Treat., 4, 283–293.